High-Resolution Structures of Human Aldose Reductase Holoenzyme in Complex with Stereoisomers of the Potent Inhibitor Fidarestat: Stereospecific Interaction between the Enzyme and a Cyclic Imide Type Inhibitor

Ossama El-Kabbani,*,† Connie Darmanin,† Mitsuru Oka,‡ Clemens Schulze-Briese,§ Takashi Tomizaki,§ Isabelle Hazemann,|| Andre Mitschler,|| and Alberto Podjarny||

Department of Medicinal Chemistry, Victorian College of Pharmacy, Monash University (Parkville Campus), 381 Royal Parade, Parkville, Vic 3052, Australia, Sanwa Kagaku Kenkyusyo Company, Ltd., 363, Shiosaki, Hokusei-cho, Inabe-gun, Mie 511-0406, Japan, Swiss Light Source at PSI, 5232 Villigen, Switzerland, and UPR de Biologie Structurale, IGBMC, CNRS INSERM ULP, 1 rue Laurent Fries, B.P. 163, 67404 Illkirch, France

Received March 20, 2004

Structure determinations of human aldose reductase holoenzyme in complex with the 2*S*4*R*-, 2*R*4*S*- and 2*R*4*R*-isomers of the potent inhibitor Fidarestat ((2*S*,4*S*)-6-fluoro-2′,5′-dioxospiro-[chroman-4,4′-imidazoline]-2-carboxamide) were carried out in order to elucidate the binding modes responsible for the differences in their inhibitory potencies. In the complex structure with the 2*R*4*S*-isomer the cyclic imide moiety formed hydrogen bonds with the side-chains of Trp111, Tyr48 and His110. In the attempt to determine the complex structure with the least potent 2*R*4*R*-isomer this ligand was not observed, and instead, the active site was simultaneously occupied by two citrate molecules (occupancies of 60% and 40%). In the case of 2*S*4*R*, the active site was occupied by a citrate molecule which anchors the 2*S*4*R*-isomer from its carbamoyl group. The structures of the complexes suggest that the differences in the interactions between the cyclic imide rings and carbamoyl groups of the compounds with residues His110, Trp111, Trp219 and Cys298 account for differences in their inhibitory potencies.

Introduction

Aldose reductase (ALR2; EC 1.1.1.21), the first enzyme of the polyol pathway of glucose metabolism, catalyzes the NADPH-dependent conversion of glucose to sorbitol. During diabetic hyperglycemia, the increased flux of glucose through the polyol pathway results in biochemical imbalances in target tissues such as nerves, lens, retina and kidneys.[1,2] Various diabetic complications such as glaucoma, neuropathies, nephropathies, retinopathies and cataracts have been attributed to these biochemical phenomena,[3,4] and as such inhibition of ALR2 represents an attractive strategy for the treatment of diabetes sufferers.[2,5] Many aldose reductase inhibitors (ARIs) have been reported in the literature; however, due to unacceptable side effects and lack of efficacy, most drug candidates were not approved for clinical use. To date only the ARI Epalrestat is successfully marketed for treatment of diabetic neuropathy in Japan, and several new potential candidates are currently undergoing clinical trials.[6,7] While there are only a few cyclic imide derivative compounds in clinical trials, the encouraging results obtained with Fidarestat ((2*S*,4*S*)-6-fluoro-2′,5′-dioxospiro[chroman-4,4′-imidazoline]-2-carboxamide) were reported recently. The results showed that Fidarestat inhibited structural and functional progressions of diabetic neuropathy[8] and halted the increase in sorbitol pathway flux in diabetic patients.[9] The recently determined 0.92 Å resolution structure of ALR2 in complex with Fidarestat (PDB entry code 1PWM) suggested that cyclic imide inhibitors initially cross the biological membrane as neutral compounds, then lose a proton and bind to the active site of the enzyme with their negative charge contributing to the tight inhibitor binding.[10] This observation is supported by the fact that the translation from *in vitro* to *in vivo* activity for this class of compounds was usually easily achieved.[11]

The overall structure of human ALR2-folds into an eight-stranded α/β-barrel with the active site located at the C-terminal end of the barrel.[12,13] The $NADP^+$ binding site is located adjacent to a hydrophobic active site pocket. Fidarestat is bound in the active site with its cyclic imide moiety entering the anion-binding site. This moiety is anchored in the active site through hydrogen bonds to the catalytic residues and van der Waals interactions with the nicotinamide ring of $NADP^+$.[10] Both carbonyl oxygen atoms are present within hydrogen bonding distances from the side-chains of Trp111 and Tyr48, while His110 forms a hydrogen bond with the negatively charged 1′-position nitrogen atom in the cyclic imide substituent. The chroman ring of Fidarestat was located within van der Waals contact distance from the side-chains of residues Trp20, Trp111, Phe122 and Trp219. The carbonyl oxygen of the carbamoyl group was hydrogen bonded to the main-chain nitrogen atom of Leu300 which lines part of the 'specificity' pocket. This interaction was suggested to be responsible for the high affinity and selectivity of Fidarestat for ALR2 over aldehyde reductase (ALR1).[14] ALR1, an enzyme responsible for the NADPH-dependent reduction of diverse aldehydes and for the metabolism of 3-deoxyglucosone and methylglyoxal which are

* To whom correspondence should be addressed. Phone: 61-3-9903-9691. Fax: 61-3-9903-9582. E-mail: Ossama.El-Kabbani@vcp.monash.edu.au.
† Monash University.
‡ Sanwa Kagaku Kenkyusyo Company.
§ Swiss Light Source at PSI.
|| CNRS INSERM ULP.

10.1021/jm0497794 CCC: $27.50
Published on Web 07/29/2004

Table 1. Data Collection and Refinement Statistics

	2*S*4*R*	2*R*4*S*	binary
Data Collection and Processing			
no. of crystals used	1	1	1
wavelength (Å)	0.79999	0.80001	0.79999
space group	$P2_1$	$P2_1$	$P2_1$
unit-cell parameters			
a, *b*, *c* (Å)	49.43, 66.89, 47.47	49.32, 66.31, 47.14	49.40, 66.78, 47.32
α, *β*, *γ* (deg)	90.0, 91.7, 90.0	90.0, 92.2, 90.0	90.0, 92.0, 90.0
resolution range (Å)	50.0−1.3	20−1.4	20−1.4
unique reflections	74739	58424	57437
$R(I)_{merg}$ (overall) (%)	4.1	3.7	3.0
$R(I)_{merg}$[a] (%)	5.4	3.7	3.9
completeness (overall) (%)	98.5	98.0	94.2
completeness[a] (%)	98.6	97.4	91.8
redundancy (overall)	4.2	4.3	4.0
redundancy[a]	4.2	3.3	2.9
$I/\sigma(I)$ (overall)	28.5	43.6	38.5
$I/\sigma(I)$[a]	24.3	21.5	7.1
Refinement			
resolution range (Å)	10−1.3	10−1.4	10−1.4
all reflections used	74738	58423	57437
size R_{free} set (%)	5	5	5
all reflections (R_{free})	(3771)	(2938)	(2872)
R_{cryst}/R_{free} (%)	17.8/21.3	19.8/24.5	16.2/19.9
R-values based on $F > 4\sigma_F$			
R_{cryst}/R_{free} (%)	17.3/20.3	19.5/23.6	15.1/18.4
protein residues	316	316	316
coenzyme	1	1	1
inhibitor	1	1	1
citrate molecules	1	0	3
water molecules	471	468	490
RMS Deviations			
bonds (Å)	0.011	0.009	0.011
angles (deg)	1.93	2.18	2.05
dihedrals (deg)	11.20	10.98	11.60
Ramachandran Plot			
residues in most favored regions (%)	90.3	90.0	91.0
residues in additional allowed regions (%)	9.7	10.0	9.0
Estimated Coordinate Error			
Luzzati mean error (Å)	0.075	0.100	0.066
Mean *B* Factor (Å^2)			
protein	11.9	15.8	14.9
$NADP^+$	5.8	8.7	8.2
inhibitor	9.4	23.8	−
citrate 1	16.2	−	24.3
citrate 2	−	−	17.7
citrate 3	−	−	17.4

[a] Data in the highest resolution shell is given in parentheses for 2*S*4*R*, 2*R*4*S* and binary between 1.37 and 1.3 Å, 1.45−1.4 Å and 1.46−1.4 Å, respectively.

intermediates for the formation of advanced glycation end products (AGEs), shares 65% sequence identity with ALR2.[15−19] Both ALR1 and ALR2 belong to the aldo-keto reductase superfamily, and the close similarities in their sequences and 3-D structures make it difficult to develop inhibitors specific only to ALR2. The least conserved residues in the two enzymes are located in the C-terminal loop which lines the hydrophobic region of the active site called the 'specificity' pocket.[12,20]

In this study the 3-D structural information obtained at high resolution from the ALR2-complexes with Fidarestat and its isomers, complemented by molecular modeling, provided an insight into the role of stereospecificity in aldose reductase inhibition, an observation which may aid the development of inhibitors that are more specific to ALR2. The chemical structures of Fidarestat (2*S*4*S*) and its isomers 2*S*4*R*, 2*R*4*R* and 2*R*4*S* are shown in Scheme 1.

Scheme 1

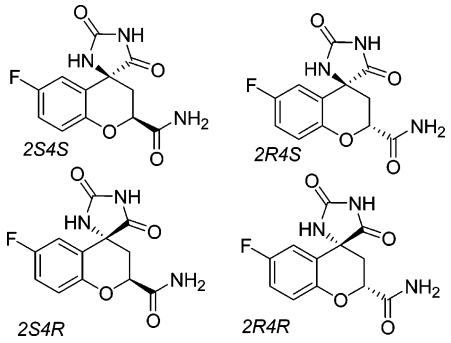

Results and Discussion

X-ray Crystallography. The structures of the holoenzyme in complex with the 2*S*4*R*- and 2*R*4*S*-isomers of Fidarestat and by itself (binary complex) were

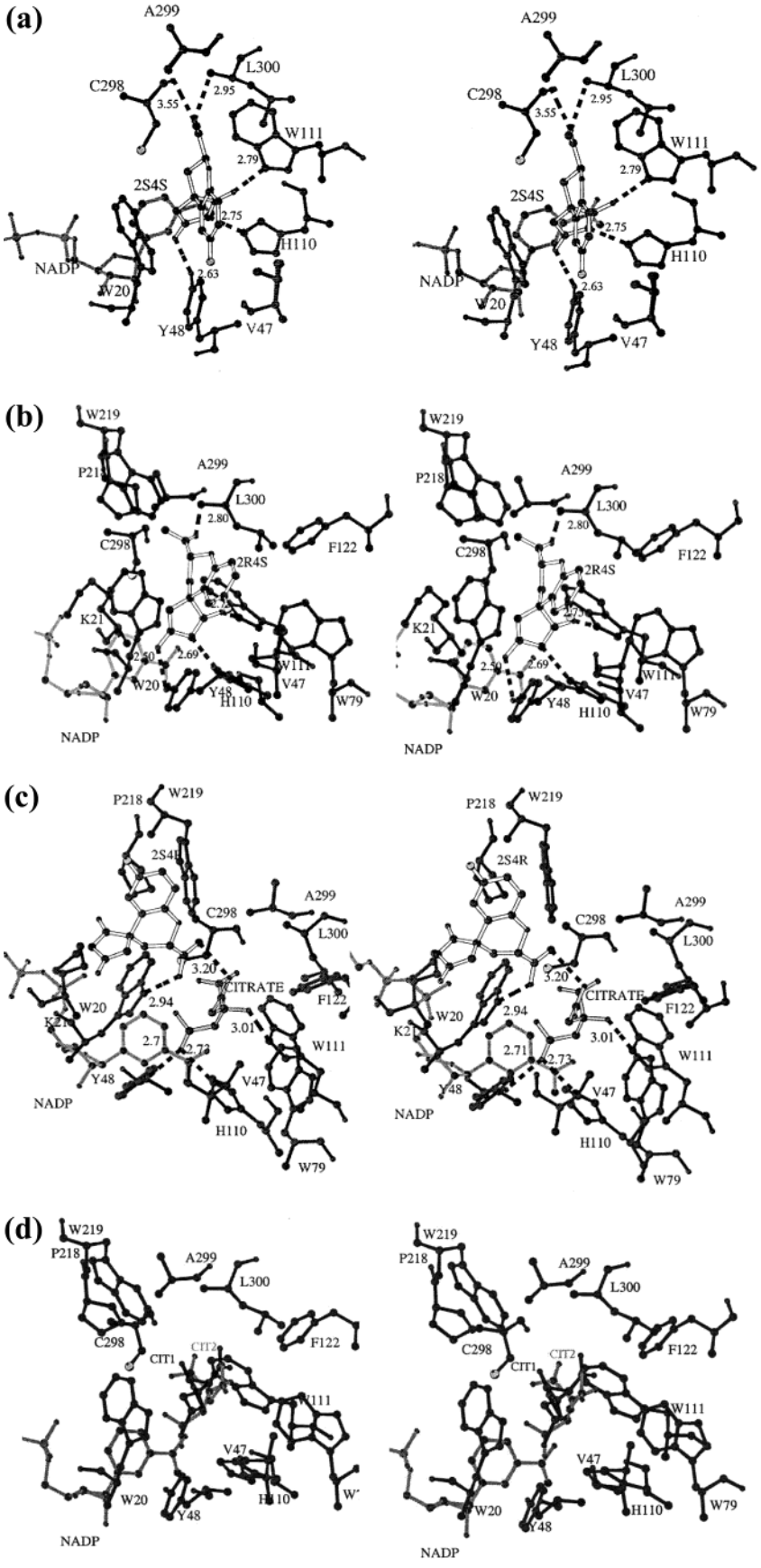
(a)
A299
L300
C298
3.55
2.95
W111
2.79
2S4S
2.75
H110
NADP
2.63
W20
Y48
V47
(b)
W219
P218
A299
L300
2.80
C298
F122
2R4S
K21
2.50
2.69
W111
W20
Y48
H110
V47
W79
NADP
(c)
P218
W219
2S4R
A299
C298
L300
3.20
CITRATE
F122
W20
2.94
K21
3.01
2.7
2.73
W111
Y48
V47
NADP
H110
W79
(d)
W219
P218
A299
L300
C298
F122
CIT1
CIT2
W111
V47
W20
Y48
H110
NADP

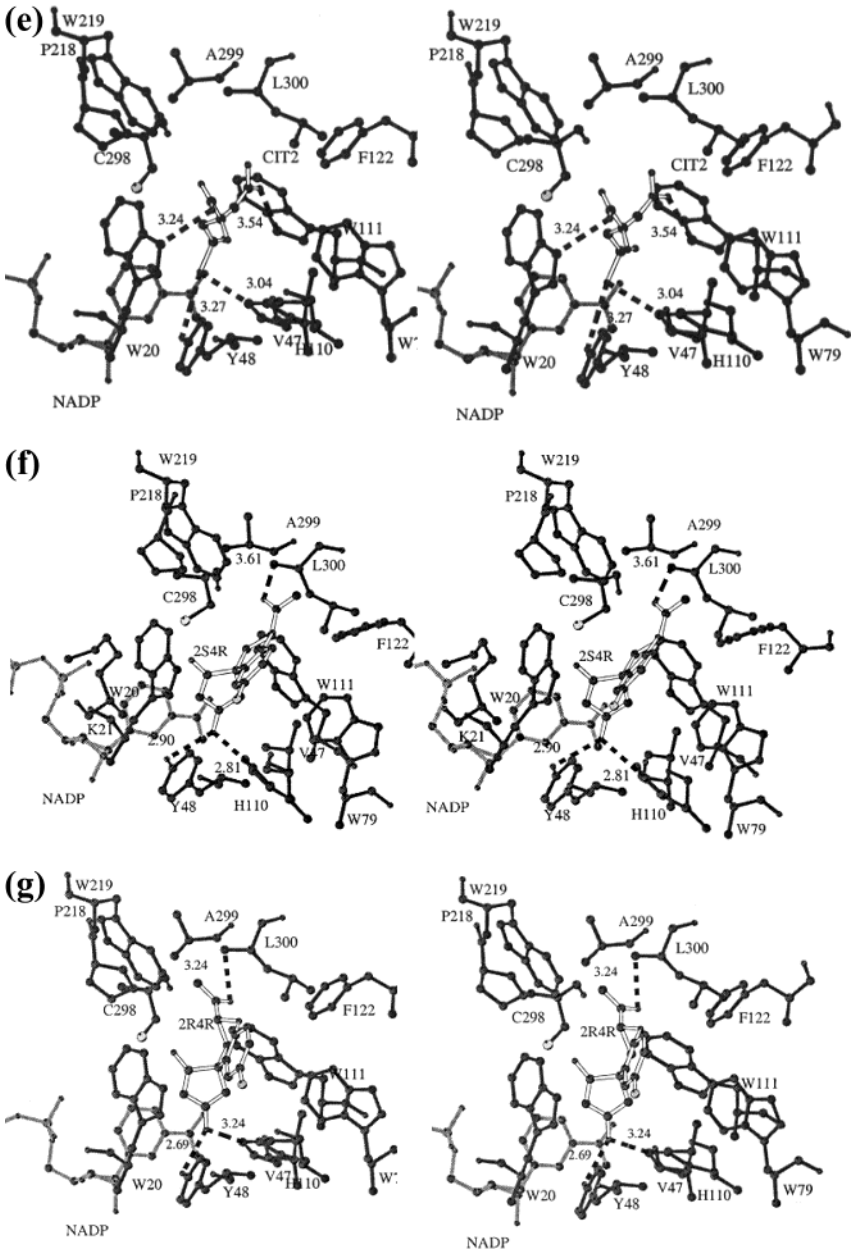

Figure 1. Stereodiagrams showing Fidarestat (2*S*4*S*), citrate molecules and the isomers (2*R*4*S*, 2*S*4*R* and 2*R*4*R*) bound to the active site of ALR2. Residues within 4 Å and hydrogen bonds as dashed lines with distances given in angstroms are shown. (a) Fidarestat (2*S*4*S*), (b) 2*R*4*S*, (c) 2*S*4*R* and citrate, (d) Binary complex with the two bound citrates, (e) Binary complex excluding the citrate conserved in the 2S4R for sake of clarity, (f) 2*S*4*R* modeled into the active site, and (g) 2*R*4*R* modeled into the active site. Figures were prepared using MOLSCRIPT.[33]

determined at maximum resolutions between 1.4 Å and 1.3 Å, with final R_{cryst} and R_{free} values between 16.3% and 19.8%, and 20.1% and 24.5%, respectively (Table 1). The asymmetric unit consisted of 316 amino acids, one $NADP^+$ coenzyme, one isomer in the case of 2*S*4*R* and 2*R*4*S*, one citrate molecule in the complex with 2*S*4*R*, three citrate molecules in the case of the binary complex and between 471 and 491 solvent molecules. A ϕ,ψ plot of main-chain torsion angles placed approximately 91% and 9% of the ALR2 residues in the most favored and additional allowed regions, respectively.[21,22] The statistics for stereochemistry and geometry of the final models are shown in Table 1.

Stereodiagrams of Fidarestat and the 2*S*4*R*-, 2*R*4*R*- and 2*R*4*S*-isomers bound to the active site of ALR2 are presented in Figure 1. As previously observed in the crystal structure of ALR2 in complex with Fidarestat,[10] the 2*R*4*S*-isomer is bound to the active site with its cyclic imide moiety entering the anion-binding site. The carbonyl oxygen atoms are present within hydrogen bonding distances from the NE1 atom of Trp111 (2.75 Å) and the OH group of Tyr48 (2.50 Å). His110 forms a hydrogen bond with the 1′-position nitrogen atom in the cyclic imide substituent (2.69 Å). In the 2*S*4*R* complex structure the active site is occupied by a citrate which anchors the 2*S*4*R* molecule from its carbamoyl group through a hydrogen bonding interaction (3.20 Å). An additional hydrogen bond is formed between the carbamoyl group of the 2*S*4*R* molecule and Trp20 (2.94 Å). In the binary complex structure, two citrate molecules occupy the active site simultaneously (occupancies of 60% and 40%). The orientation of the citrate molecule in the 2*S*4*R* is conserved as in the binary complex structure (60% occupancy) and is located within hydro-

gen bonding distances from the side-chains of residues Tyr48 (2.71 Å), His110 (2.73 Å) and Trp111 (3.01 Å). The second citrate occupying the active site of the binary complex (40% occupancy) interacts with Trp20 (3.24 Å), Tyr48 (3.27 Å), His110 (3.04 Å) and Trp111 (3.54 Å). The second citrate was clearly identified at subatomic resolution by T. R. Schneider and collaborators (paper in preparation). Both the modeled 2*R*4*R*- and 2*S*4*R*-isomer in the active site form hydrogen bonds with Tyr48 (2.69 Å and 2.90 Å, respectively) and His110 (3.24 Å and 2.81 Å, respectively). The hydrogen bond observed between Trp111 and both Fidarestat (2.79 Å) and the 2*R*4*S*-isomer (2.75 Å) is missing in the 2*R*4*R* and 2*S*4*R* models.

Unlike the binding of Minalrestat, an ARI which also belongs to the cyclic imide class of inhibitors,[10] the binding of Fidarestat and its isomers to ALR2 does not induce a conformational change in the side-chain of Leu300, a residue which lines part of the 'specificity' pocket. The carbamoyl group of Fidarestat forms a hydrogen bond with the main-chain nitrogen atom of Leu300. This residue is a Pro in ALR1, and its inability to form a hydrogen bond with the inhibitor was attributed to the much higher selectivity of Fidarestat for ALR2.[14] Comparisons between the structures of Fidarestat and its isomers (Figure 1) show that the interaction of the carbamoyl group with the C-terminal loop residues is not conserved. While the hydrogen bond (2.95 Å) between the carbamoyl group of Fidarestat and the main-chain nitrogen atom of Leu300 is conserved in the 2*R*4*S* (2.80 Å) and the modeled 2*R*4*R* (3.24 Å) and 2*S*4*R* (3.61 Å) structures, the long hydrogen bond with the main-chain nitrogen atom of Ala299 (3.55 Å) is missing. This is not surprising when considering that there are no induced fit conformational changes in the residues lining the binding site. Furthermore, induced rotations in the carbamoyl groups may occur to accommodate the compounds into the binding site, as suggested by the close contacts between the side-chains of Trp219 and Cys298 and the carbamoyl groups of Fidarestat (3.61 Å and 3.29 Å, respectively), 2*S*4*R*- (3.25 Å and 3.60 Å, respectively), 2*R*4*S*- (3.00 Å and 2.98 Å, respectively), and 2*R*4*R*-isomers (3.52 Å and 3.73 Å, respectively). In an earlier study,[14] the modeling of the 2*R*4*S*-isomer and the crystal structure of the ALR2−Fidarestat complex determined at 2.8 Å resolution also suggested that the two compounds bind to ALR2 in a similar manner and that the stereochemistry of the carbamoyl group might have an influence on their affinity to the enzyme. However, the close contacts of the 2*R*4*S*-isomer with Trp219 and Cys298, and the nonconserved long hydrogen bond with Ala299, were not predicted.

The structures of the ALR2 complexes show differences in the interactions between the cyclic imide and carbamoyl groups of the compounds and the residues lining the binding site. For comparisons, and to examine the correlation between the electrostatic component of the binding energy and the binding constants measured in solution for the compounds, an estimation of the electrostatic interactions between the active site residues Tyr48, His110 and Trp111 and the polar heads of the inhibitors was obtained from molecular modeling. The electrostatic component of the binding energy (ΔH) and the in vitro potency of the compounds (IC_{50}) are listed in Table 2. The calculated binding energies ranged from −11 to −30 kcal/mol with corresponding IC_{50} values ranging from 0.035 to 40 μM. The similarity in the IC_{50} values of Sorbinil ($IC_{50} = 0.90$ μM), an ARI that is missing the carbamoyl group, and the 2*R*4*S*-isomer ($IC_{50} = 0.54$ μM) is in agreement with the earlier proposal that the stereochemistry of the carbamoyl group influences the affinity of the compounds.[14,23]

Table 2. Comparison of ALR2 Inhibitor Binding Constants[a]

inhibitor	IC_{50}, μM	ΔH (kcal/mol)
Fidarestat	0.035	−30
2*R*4*S*	0.57	−20
2*S*4*R*	11	−16
2*R*4*R*	40	−11

[a] The IC_{50} values (binding constants measured in solution) of the compounds against ALR2 were reported by Yamaguchi *et al.* (1994). ΔH values (Intermolecular binding enthalpies) were calculated between the catalytic residues Tyr48, His110 and Trp111 of ALR2 and the bound compounds.

Effects of the *R*- and *S*-Configurations on Inhibitor Binding. The clear electron density corresponding to the cyclic imide moiety of the 2*R*4*S*-isomer bound to the active site indicates that the compound is anchored mainly through its polar head. The electrostatic interactions are conserved in the structures of the complexes with Fidarestat (2*S*4*S*) and the 2*R*4*S*-isomer where the side-chains of Tyr48 and Trp111 form hydrogen bonds with the carbonyl oxygen atoms and the side-chain of His110 is hydrogen bonded to the negatively charged nitrogen atom at the 1′-position, contributing to the tight inhibitor binding (IC_{50} values equal to 0.035 μM and 0.57 μM, respectively).[23] In case of the complex structures with the modeled 2*R*4*R*- and 2*S*4*R*-isomers the hydrogen bonds with the side-chain of Trp111 and the negatively charged nitrogen atom at the 1′-position are missing, and therefore weaker binding of the compounds would be expected (IC_{50} values equal to 40 μM amd 11 μM, respectively).[23] Moreover, the short contacts between the carbamoyl group of the 2*R*4*S*-isomer (present in the *R*-configuration) and Trp219 and Cys298 compared to Fidarestat (2*S*4*S*) may contribute to the weaker binding of the former compound (3.00 Å and 2.98 Å versus 3.61 Å and 3.29 Å, respectively).

The binding of the citrate molecule to the active site of the enzyme interferes with the binding of the 2*S*4*R*- and 2*R*4*R*-isomers (cyclic imide ring in the *R*-configuration) in the crystal structure. In case of the 2*S*4*R*-isomer the carbamoyl group in the *S*-configuration is positioned to form a hydrogen bond with the citrate molecule and the side-chain of Trp20. Unlike Fidarestat and 2*R*4*S*, the 2*S*4*R*-isomer in the crystal structure is anchored from its carbamoyl group and has no interactions with the active site residues Tyr48, His110 and Trp111.

The correlation between the calculated binding energies and in-solution binding constants (IC_{50}) for the compounds suggests that the holoenzyme essentially differentiates between the *S*- and *R*-configurations for both the cyclic imide (4-position) and carbamoyl (2-position) groups. The cyclic imide ring in the *S*-configuration (2*S*4*S*- and 2*R*4*S*-isomers) is optimally located for the formation of a hydrogen bonding network with Tyr48, His110 and Trp111. While the carbamoyl group in the *S*-configuration (2*S*4*S*-isomer) forms favored stereospecific interactions with Trp219 and the C-

terminal residues lining the binding site (Cys298, Ala299 and Leu300), the tight hydrogen bonding network between the active site residues (Tyr48, His110 and Trp111) and the cyclic imide ring in the *S*-configuration is mostly responsible for the stronger binding of Fidarestat (2*S*4*S*) and the 2*R*4*S*-isomer to ALR2.

Summary

The *R*- and *S*-configurations for both the cyclic imide and carbamoyl groups were used as probes to investigate the stereospecific interactions with ALR2 since Fidarestat (2*S*4*S*) was shown to bind to the active site,[10] and with the exception of the free rotation of the carbamoyl group, the compounds are conformationally restricted. The compounds are anchored through their cyclic imide rings to the active site and the hydrogen bonding network between the active site residues Tyr48, His110 and Trp111 and the cyclic imide ring in the *S*-configuration is responsible for firmly anchoring the compounds. The cyclic imide in the *R*-configuration, on the other hand, does not form a tight hydrogen bonding network with the active site residues, thus missing the important electrostatic interactions with the negatively charged nitrogen atom at the 1′-position and the side-chain of Trp111. While the hydrogen bond between the carbamoyl group and the main-chain nitrogen atom of Leu300 is conserved, the short contacts between Trp219 and Cys298 and the carbamoyl group in the *R*-configuration (2*R*4*S*) makes it less favorably located compared to the *S*-configuration (2*S*4*S*). The correlation between the binding energies (ΔH) and in-solution binding constants (IC_{50}) for the compounds confirms our proposal that hydrogen bonding interactions with the cyclic imide ring and favored van der Waals contacts with the carbamoyl group account for the stronger binding of the *S*-isomers to the enzyme as well as the 1143-fold difference in inhibitory potency between Fidarestat (2*S*4*S*) and the 2*R*4*R*-isomer.

Experimental Section

Expression and Purification of Human ALR2. The open reading frame of the human ALR2 gene (Accession Gene Bank/EMBL Data Bank Number J05017) was amplified by PCR from cDNA[24] and cloned into T7 RNA polymerase-based vector pET15b (Novagen). Expression of hexahistidine tagged protein in *Escherichia coli* strain BL21 (DE3) (Novagen) was induced by IPTG (Euromedex) during a 3-h period at 37 °C. The pellet from a 4-L culture was disrupted by sonication and centrifuged. The supernatant was loaded onto a Talon metal-affinity column (Clonetech). After thrombin cleavage of the hexahistidine extension, the detagged protein was loaded onto a DEAE Sephadex A-50 column (Pharmacia) and eluted with a NaCl gradient.[24]

Crystallization. Prior to crystallization, human ALR2 at 16 mg/mL in 50 mM ammonium citrate buffer (pH 5) was mixed with $NADP^+$ and inhibitor (molar ratio of ALR2:$NADP^+$:inhibitor was 1:2:2.5). The binary and ternary ternary complexes were crystallized using the vapor-diffusion method. The ALR2/$NADP^+$/inhibitor solution was mixed with an equal volume of 15% (w/v) poly(ethylene glycol) (PEG) 6000 in 50 mM ammonium citrate buffer (pH 5) and 10 μL hanging droplets were placed above a well solution (1 mL) containing 20% PEG 6000 and 120 mM ammonium citrate. Crystals were grown at 277 K, transferred into a stabilization solution (25% PEG 6000), then into a cryoprotecting solution (40% PEG 6000) and dipped into liquid nitrogen. The effect of the crystallization pH on the protonation states of the inhibitor and the active site residues of ALR2 was discussed, and a mechanism for inhibitor binding was proposed in an earlier study based on the ultrahigh-resolution structure of the ALR2−Fidarestat complex.[10]

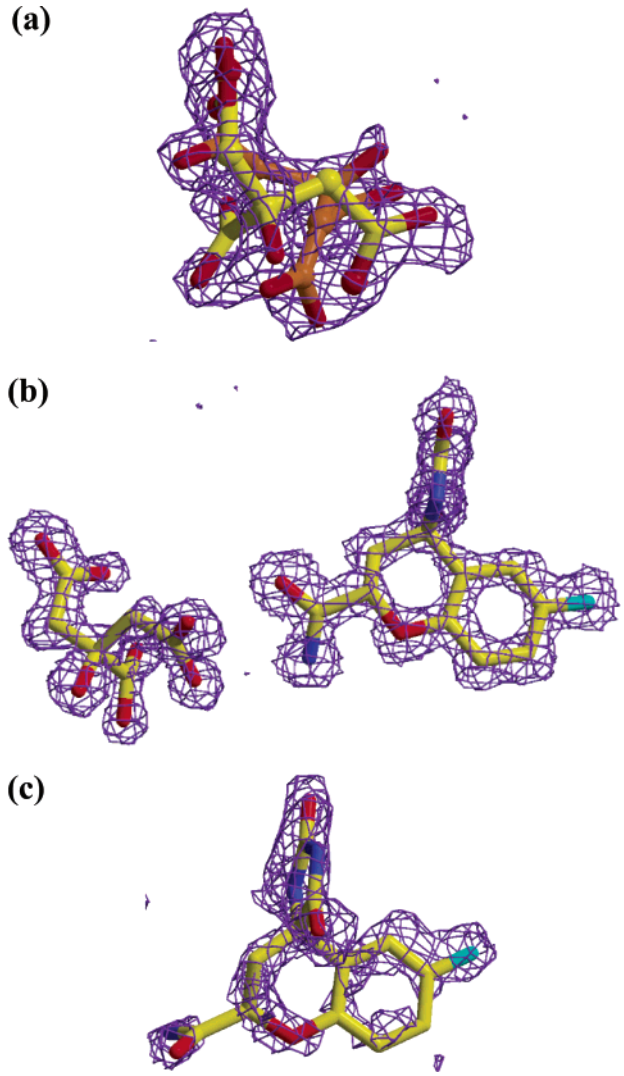

Figure 2. Omit electron density maps ($F_o - F_c$) calculated with a 2.5 − σ cutoff superimposed on the final models of the Fidarestat isomers (2*S*4*R* and 2*R*4*S*) and citrate molecules. (a) Binary complex citrates at 1.4 Å resolution, (b) 2*S*4*R*-isomer and citrate at 1.3 Å resolution, and (c) 2*R*4*S*-isomer at 1.4 Å resolution.

X-ray Data Collection and Processing. The binary and ternary complexes with 2*S*4*R*- and 2*R*4*S*-isomers crystallized in the monoclinic $P2_1$ space group, with unit cell parameters $a = 49.43$ Å, $b = 66.89$ Å, $c = 47.47$ Å and $\beta = 91.7°$ (at 100 K). There was one monomer per asymmetric unit, consisting of 316 amino acid residues. The solvent content was estimated to occupy 34.6% of the unit cell volume.[25] Crystals were initially checked at ESRF, beamline BM30. Almost complete synchrotron data sets were collected at the Swiss Light Source beamline ×06SA from each isomer-complexed crystal and processed using the programs *HKL2000* and SCALEPACK.[26] The exposure time (1−15 s), oscillation range (0.2−1°) and crystal-detector distance (115 mm) were adjusted to optimize each data set. Crystals proved resistance to radiation damage at 100 K allowing the measurements of 2 × 180° zones in reciprocal space for near complete data sets between low and high-resolution ranges. Data collection and processing statistics are shown in Table 1.

Structure Refinement. The atomic coordinates of the human ALR2−Fidarestat complex (PDB entry code 1PWM), which crystallized in the same space group with similar unit cell parameters, were used to solve the structures of the binary and ternary complexes with the 2*R*4*S*- and 2*S*4*R*-isomers.

Crystallographic refinement involved repeated cycles of conjugate gradient energy minimization, simulated annealing and temperature factor refinement.[27] Amino acid side-chains were fitted into $2F_o - F_c$ and $F_o - F_c$ electron density maps. The final $F_o - F_c$ maps (Figure 2) indicated clear electron densities for the 2*S*4*R*-isomer and for the cyclic imide moiety of the 2*R*4*S*-isomer. There was no electron density corresponding to the 2*R*4*R*-isomer, and instead, the active site was simultaneously occupied with two citrate molecules. In the 2*S*4*R* complex structure a citrate molecule was located bound into the active site. Water molecules were fitted into difference maps, and final cycles of conjugate gradient refinement were carried out using the *SHELX* program package.[28] The programs *TURBO-FRODO*[29] and *XtalView/Xfit*[30] were used for fitting the models into the electron density. The difference electron density maps allowed the identification of multiple conformations for several amino acid residue side-chains. Refinement statistics are presented in Table 1.

Molecular Modeling Calculations. To obtain a picture of the binding conformation of the 2*R*4*R*- and 2*S*4*R*-isomers the compounds were docked in the active site of the binary complex based on the orientation of Fidarestat in the crystal structure.[10] Energy minimization calculations were carried out on the structures of the complexes using the Discover 2.7 package (Biosym Technologies, San Diego, CA), on an O2 (R12000) workstation (Silicon Graphics, Mountain View, CA) following established procedures found to be effective in examining conformational space with a protein−ligand complex.[31,32] Arginine, lysine, aspartate and glutamate amino acids were charged while the histidines were uncharged, with hydrogen atoms fixed at the Nϵ2 atom. The detailed structural information revealed from the atomic resolution refinement of the ALR2 holoenzyme complexed with Fidarestat[10] was considered during the modeling calculations. The imidazole ring of His110 was protonated at the Nϵ2 atom position and formed a hydrogen bond with the negatively charged 1′-position nitrogen atom of the cyclic imide rings of the inhibitors. The constant valence force field incorporating the simple harmonic function for bond stretching and excluding all nondiagonal terms was used (cutoff distance of 31 Å). Calculations were done using the steepest descents and conjugate gradients algorithms (down to a maximum atomic root-mean-square derivative of 10.0 kcal/Å and 0.01 kcal/Å, respectively). The structures were visualized by using InsightII and the contribution of the active site residues Tyr48, His110 and Trp111, adjacent to the compounds, to the binding energy in the ALR2 complex was calculated by using Discover (Table 2).

Acknowledgment. We thank Thomas Schneider for helpful discussions, the staff of the SLS for their help in data collection, the IGBMC staff for support with purification, crystallization and computing facilities, and Jean Luc Ferrer, ESRF beamline BM30, for his help in checking crystals. This work was supported by the Australian Research Council, Sanwa Kagaku Kenkyusyo Company, Ltd., the Centre National de la Recherche Scientifique (CNRS), the collaboration CERC-CNRS, Ecos Sud, the Institut National de la Santé et de la Recherche Médicale (INSERM) and the Hôpital Universitaire de Strasbourg (H.U.S). The atomic coordinates will be deposited in the Protein Data Bank and will be released immediately upon publication.

References

(1) Costantino, L.; Rastelli, G.; Vianello, P.; Cignarella, G.; Barlocco, D. Diabetes complications and their potential prevention: aldose reductase inhibition and other approaches. *Med. Res. Rev.* **1999**, *19*, 3−23.

(2) Yabe-Nishimura, C. Aldose reductase in glucose toxicity: a potential target for the prevention of diabetic complications. *Pharmacol. Rev.* **1998**, *50*, 21−33.

(3) Kintoshita, J. H.; Nishimura, C. The involvement of aldose reductase in diabetic complications. *Diabetes Metab. Res.* **1988**, *4*, 323−337.

(4) Dunlop, M. Aldose reductase and the role of the polyol pathway in diabetic nephropathy. *Kidney Int. Suppl.* **2000**, *77*, S3−S12.

(5) Costantino, L.; Rastelli, G.; Gamberini, M. C.; Barlocco, D. Pharmacological approaches to the treatment of diabetic complications. *Exp. Opin. Ther. Pat.* **2000**, *10*, 1245−1262.

(6) Kaul, C. L.; Ramarao, P. The role of aldose reductase inhibitors in diabetic complications: recent trends. *Methods Find. Exp. Clin. Pharmacol.* **2001**, *23*, 465−475.

(7) Miyamoto, S. Recent advances in aldose reductase inhibitors: potential agents for the treatment of diabetic complications. *Expert Opin. Ther. Pat.* **2002**, *12*, 621−631.

(8) Oates, P. J.; Mylari, B. L. Aldose reductase inhibitors: therapeutic implications for diabetic complications. *Exp. Opin. Invest. Drugs* **1999**, *8*, 1−25.

(9) Pfeifer, M. A.; Schumer, M. P.; Gelber D. A. Aldose reductase inhibitors: the end of an era or the need for different trial design. *Diabetes* **1997**, *46*, S82−S89.

(10) El-Kabbani, O.; Darmanin, C.; Schneider, T. R.; Hazemann, I.; Ruiz, F.; Oka, M.; Joachimiak, A.; Schulze-Briese, C.; Tomizaki, T.; Mitschler, A.; Podjarny, A. Ulta-high-resolution drug design II: Atomic resolution structures of human aldose reductase holoenzyme complexed with Fidarestat and Minalrestat; implications for the binding of cyclic imide inhibitors. *Proteins* **2004**, *55*, 805−813.

(11) Rastelli, G.; Ferrari, A. M.; Costantino, L.; Gamverini, M. C. Discovery of new inhibitors of aldose reductase from molecular docking and database screening. *Bioorg. Med. Chem.* **2002**, *10*, 1437−1450.

(12) El-Kabbani, O.; Wilson, D.; Petrash, J. M.; Quiocho, F. A. Structural features of the aldose reductase and aldehyde reductase inhibitor-binding sites. *Mol. Vision* **1998**, *4*, 19−25.

(13) Urzhumtsev, A.; Tête-Favier, F.; Mitschler, A.; Barbanton, J.; Barth, P.; Urzhumtseva, J. F.; Biellmann, A. D.; Podjarny, A.; Moras, D. A. 'Specificity' pocket inferred from the crystal structures of the complexes of aldose reductase with the pharmaceutically important inhibitors tolrestat and sorbinil. *Structure* **1997**, *5*, 601−612.

(14) Oka, M.; Matsumoto, Y.; Sugiyama, S.; Tsuruta, N.; Matsushima, M. A potent aldose reductase inhibitor, (2*S*,4*S*)-6-Fluoro-2′,5′dioxyspiro[chroman-4,4′-imidazoline]-2-carboxamide (Fidarestat): its absolute configuration and interaction with aldose reductase by X-ray crystallography. *J. Med. Chem.* **2000**, *43*, 2479−2483.

(15) Jez, J. M.; Bennett, M. J.; Schlegel, B. P.; Lewis, M.; Penning, T. M. Comparative anatomy of the aldo-keto reductase superfamily. *Biochem. J.* **1997**, *326*, 625−636.

(16) Warren, J. C.; Murdock, G. L.; Ma, Y.; Goodman, S. R.; Zimmer, W. E. Molecular cloning of testicular 20 alpha-hydroxysteriod dehydrogenase: identity with aldose reductase. *Biochemistry* **1993**, *32*, 1401−1406.

(17) Tanimoto, T.; Nishijama, C. Molecular biology of aldose reductase. *Exp. Med.* **1991**, *9*, 541−547.

(18) Feather, M. S.; Flynn, T. G.; Munro, K. A.; Kubiseski, T. J.; Walton, D. J. Catalysis of reduction of carbohydrate 2-oxoaldehydes (osones) by mammalian aldose reductase and aldehyde reductase. *Biochim. Biophys. Acta* **1995**, *1244*, 10−16.

(19) Ratliff, D. M.; Van der Jagt, D. J.; Eaton, R. P.; Van der Jagt, D. L. Increased levels of methylglyoxal-metabolizing enzymes in mononuclear and polymorphonuclear cells from insulin-dependent diabetic patients with diabetic complications: aldose reductase, glyoxalase I, and glyoxalase II-a clinical research center study. *J. Clin. Endocrinol. Metab.* **1996**, *81*, 488−492.

(20) El-Kabbani, O.; Old, S. E.; Ginell, S. L.; Carper, D. A. Aldose and aldehyde reductases: structure−function studies on the coenzyme and inhibitor-binding sites. *Mol. Vision* **1999**, *5*, 20−26.

(21) Laskowski, R. A.; MacArthur, M. W.; Moss, D. S.; Thornton, J. M. PROCHECK: a program to check the stereochemical quality of protein structures. *J. Appl. Crystallogr.* **1993**, *26*, 283−291.

(22) Ramachandran, G. N.; Sasisekharan, V. Conformation of proteins and polypeptides. *Adv. Protein Chem.* **1968**, *23*, 283−437.

(23) Yamaguchi, T.; Miura, K.; Usui, T.; Unno, R.; Matsumoto, Y.; Fukushima, M.; Mizuno, K.; Kondo, Y.; Baba, Y.; Kurono, M. Synthesis and aldose reductase inhibitory activity of 2-substituted-6-fluoro-2,3-dihydrospiro [4H-1-benzopyran-4, 4′-imidazolidine]-2′, 5′-diones. *Arzneim.-Forsch./Drug Res.* **1994**, *44*, 344−348.

(24) Chung, S.; La Mendola, J. Cloning and sequence determination of human placental aldose reductase gene. *J. Biol. Chem.* **1989**, *264*, 4775−14777.

(25) Matthews, B. W. Solvent content of protein crystals. *J. Mol. Biol.* **1968**, *33*, 491−497.

(26) Otwinowski, Z.; Minor, W. Processing of X-ray diffraction data collected in oscillation mode. *Methods Enzymol.* **1997**, *276*, 307−326.
(27) Brünger, A. T.; Krukowski, A.; Erickson, J. W. Slow-cooling protocols for crystallographic refinement by simulated annealing. *Acta Crystallogr. A* **1990**, *46*, 585−593.
(28) Sheldrick, G.; Schneider, T. SHELXL: high-resolution refinement. *Methods Enzymol.* **1997**, *277*, 319−343.
(29) Roussel, A.; Cambillau, C. TURBO-FRODO molecular graphics program. In *Silicon Graphics Geometry Partner Directory*; Silicon Graphics: Mountain View, CA, 1989, pp 77−78.
(30) McRee, D. E. XtalView/Xfit—A versatile program for manipulating atomic coordinates and electron density. *J. Struct. Biol.* **1999**, *125*, 156−165.
(31) Darmanin, C.; El-Kabbani, O. Modelling studies of the active site of human sorbitol dehydrogenase: an approach to structure-based inhibitor design of the enzyme. *Bioorg. Med. Chem. Lett.* **2001**, *11*, 3133−3136.
(32) Darmanin, C.; El-Kabbani, O. Modelling studies on the binding of substrate and inhibitor to the active site of human sorbitol dehydrogenase. *Bioorg. Med. Chem. Lett.* **2000**, *10*, 1101−1104.
(33) Kraulis, P. J. MOLSCRIPT: A program to produce both detailed and schematic plots of protein structures. *J. Appl. Crystallogr.* **1991**, *24*, 946−950.

JM0497794